

Theory of the extended x-ray absorption fine structure

P. A. Lee

Department of Physics, University of Washington, Seattle, Washington 98195
and Bell Laboratories,† Murray Hill, New Jersey 07974*

J. B. Pendry

The Cavendish Laboratory, University of Cambridge, Cambridge, England

(Received 29 October 1974)

The extended x-ray absorption fine structure is a consequence of the modification of the photoelectron final state due to scattering by the surrounding atoms. We present a theory of the absorption fine structure starting from theoretically obtained electron-atom scattering phase shifts. The electron scattering is treated using a spherical wave expansion which takes into account the finite size of the atoms. Multiple-scattering effects are included by classifying multiple-scattering paths by their total path lengths. Their effects are quite large but appear to make quantitative but not qualitative changes on the single-scattering contribution. The exceptional case is the fourth shell in fcc or bcc structure, where it is shadowed by the first-shell atom and is profoundly affected by forward scattering due to the first shell. This may account for the anomaly observed experimentally at the fourth-shell radius in metals. A detailed numerical calculation is carried out for copper and is shown to agree quite well with experiment.

I. INTRODUCTION

It has been known for over 40 years that the x-ray absorption coefficient in matter exhibits oscillations as a function of energy above threshold.¹ A typical such spectrum is shown in Fig. 1 for copper. Recently there has been a renewal of interest in the subject after the work of Sayers, Stern, and Lytle,² who pointed out that such extended x-ray absorption fine structure (EXAFS) can be used to obtain structural information of solids. Their suggestion is first to examine the function $\chi(\omega)$ obtained by isolating the purely oscillatory part of the absorption coefficient in Fig. 1 and normalizing it with respect to the smooth background. The next step is to plot χ versus the photoelectrons wave vector k , which is defined as

$$\hbar k = \{2m[\hbar(\omega - \omega_T) + E_0]\}^{1/2}, \quad (1.1)$$

where ω_T is the threshold frequency and E_0 is the Fermi energy. Since we are interested in an energy range of 50 to 2000 eV above threshold, k is not very sensitive to the choice of E_0 . According to the theory of Sayers *et al.* $\chi(k)$ is a superposition of terms of the form $\sin(2kR_j)$, where R_j measures the distance to the neighbors surrounding the excited atom. The Fourier transform

$$F(r) = \int \frac{dk}{2\pi} e^{-i2kr} \chi(k) \quad (1.2)$$

should peak at the distances $r = R_j$ and should provide information on the structure of the solid. Since this technique is particularly sensitive to the local environment of atoms and does not require the use of single crystals, it is especially useful

in the study of disordered systems² and complex materials, such as catalysts.³ Unlike conventional x-ray diffraction the surroundings of each constituent atom can be separately studied by looking at the respective absorption edge.

The phenomenon of EXAFS is sufficiently complex that one would like to gain some understanding of EXAFS in crystalline materials where the structure is well known before one can apply the technique to complex materials with confidence. Recent work⁴ has already shown that even in crystals there are observations that cannot be explained in terms of the simple theory discussed in Ref. 2. As an example we show in Figs. 2 and 3 the Fourier transforms of the absorption rates for crystalline Ge and Cu. It is expected that such transforms should peak at distances corresponding to the shell distances as marked by the arrows. While this description works very well for Ge, for Cu it is found that the fourth shell appears to have turned upside down.⁵ This kind of phase reversal has been observed for a variety of metals. It is the object of this paper to perform a calculation of the EXAFS spectrum starting from the atomic phase shifts. Our calculation will relax several of the assumptions made by the theory in Ref. 2. Since the most interesting and extensive data are available for Cu we have carried through the calculation for crystalline copper. It is our hope that our work will throw some light on the observed difference between metals and semiconductors, and serve to indicate under what circumstances a more accurate theory is called for.

The experimentally measured quantity is the contribution to the x-ray absorption coefficient due

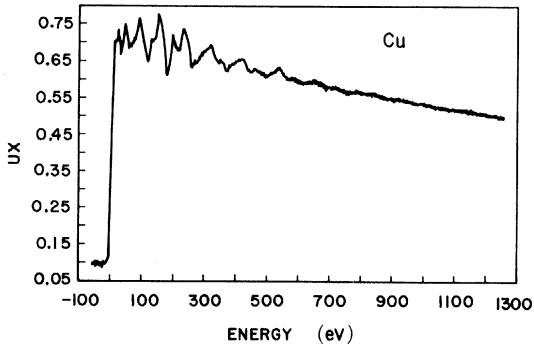


FIG. 1. k -shell absorption coefficient UX of copper vs the x-ray photon energy. The zero of energy is chosen at the K edge.

to the excitation of a deep core level. This can be related in a straightforward manner to the transition rate per unit photon flux τ^{-1} which in the dipole approximation is given by the Golden Rule:

$$\frac{1}{\tau} = \frac{2\pi}{\hbar} \sum |\langle f | e \vec{\epsilon} \cdot \vec{r} | i \rangle|^2 \delta(E_i + \hbar\omega - E_f), \quad (1.3)$$

where $\vec{\epsilon}$ is the polarization vector of the electric field. The initial state is the core state plus a Fermi sea whereas the final state consists of a core hole and an excited electron. For simplicity we assume that the core state is an s state so that the final electron state must have p symmetry. If the atom were isolated then the final electron state is simply an outgoing wave, and τ^{-1} should be a

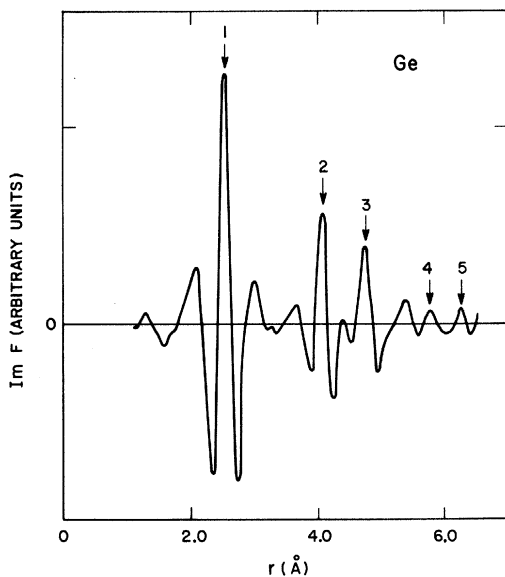


FIG. 2. Imaginary part of the Fourier transform of $\chi(k)$ plotted vs r for crystalline Ge.

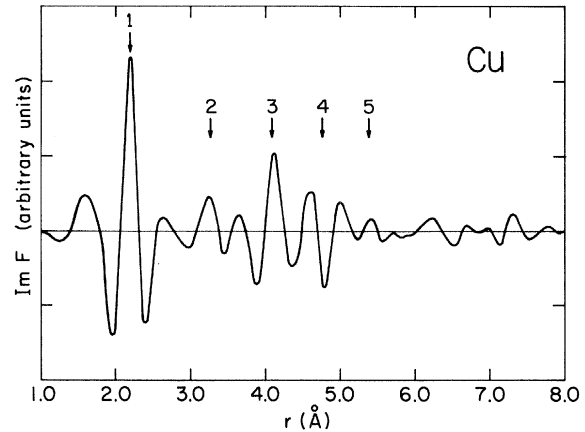


FIG. 3. Imaginary part of the Fourier transform of $\chi(k)$ plotted vs r for Cu.

smooth function of the photon energy above threshold. In a solid the atom is surrounded by other atoms and the outgoing wave function will be diffracted by the neighboring atoms, resulting in incoming waves which modify the final state. Based on these physical ideas Sayers, Stern, and Lytle² have written down the following expression for the normalized oscillatory part of the absorption rate $\chi(k)$:

$$\begin{aligned} \chi(k) &= \tau^{-1} / \tau_0^{-1} - 1 \\ &= \frac{1}{k} \sum_j \frac{N_j}{R_j^2} S(k) \sin[2kR_j + 2\delta_1'(k)] e^{-2\sigma_j^2 k^2} e^{-\gamma R_j}, \end{aligned} \quad (1.4)$$

where τ_0^{-1} is the smooth background absorption rate corresponding to the isolated atom. The function $S(k)$ is the backscattering amplitude from each of the N_j neighboring atoms in the j th shell located at a distance R_j away from the central excited atom. The factor $e^{-2\sigma_j^2 k^2}$ is a Debye-Waller factor to take into account thermal vibration or the atomic position and $e^{-\gamma R_j}$ describes the decay of the photoelectron. The phase $\delta_1'(k)$ is the $l=1$ phase shift of the photoelectron caused by the potential of the absorbing atom. The basic assumptions in the derivation of Eq. (1.4) are as follows: (i) The outgoing wave can be approximated by $(-ie^{i(kr+\delta_1^l)/k\gamma})Y_{1m}(\Omega)$. The factor of $-i$ which is responsible for the sin instead of cos in Eq. (1.4) is needed for a proper definition of the phase shift so that the phase shift is zero in the absence of a potential [see Eq. (A10)]. (ii) A small-atom approximation has been employed in the sense that the atomic radius is small enough for the curvature of the incident wave to be neglected. The incident wave on the neighboring atom is then approximated by a plane wave. (iii)

Only single scattering by the surrounding atoms is included.

Within these assumptions the $\sin(2kR_j + 2\delta'_1)$ factor simply arises from the phase-change experience by the wave function on its outward and return trips, plus the phase shift $\delta'_1(k)$ due to the central atom. What Sayers *et al.* observed is that if one makes the additional assumption (iv) that $\delta'_1(k)$ is a linear function of k , i. e.,

$$\delta'_1(k) = \alpha k + \delta_0, \quad (1.5)$$

then the Fourier transform of $\chi(k)$ will be sharply peaked about $2(R_j + \alpha)$. The Fourier transform then provides information on the relative position of the shells. It is further argued that if Eq. (1.5) is correct and α depends only on the central atom, then α can be determined from a crystalline sample and then the absolute shell distances can be obtained for unknown structures, of amorphous samples as well as compounds involving other types of neighboring atoms.

In the present work we relax some of the assumptions made in Ref. 2. However, we shall stay within a single-particle description and make the muffin-tin approximation for the atomic potential. Many-body effects are included via a self-energy correction to the Green's function which gives the electron a finite coherent path length. However, more subtle many-body effects and band-structure details are expected to be important near threshold. Hence we expect our theory to be applicable beginning roughly 20 or 50 eV above threshold. This coincides with the experimentally interesting region for EXAFS. The muffin-tin approximation should be adequate for computing scattering by neighboring atoms. However, to treat the central atom adequately one would have to worry about the time-dependent screening and relaxation of the core hole. This problem we will not deal with here. As discussed in more detail in Sec. II, we have simply calculated the central-atom phase shift $\delta'_1(k)$ assuming an ionized atom screened by conduction electron. The approximation of a neutral atom is probably one of the limiting factors in the accuracy of the theory.

The plan of the paper is as follows. In Sec. II we will discuss the calculation of the atomic phase shift. The phase shift will then be used to calculate the absorption rate, including only a single backscattering by a neighboring atom. This calculation then relaxes assumptions (i) and (ii) and within our rather crude treatment of the central atom also serves to check assumption (iv). In Sec. III we will extend the calculation to include multiple scattering by the surrounding atoms. Section IV is the conclusion.

II. SINGLE-SCATTERING THEORY

The scattering of electrons by atoms with electron energy up to about 500 eV has received considerable attention recently, most of the work being connected with the theory of low-energy-electron diffraction (LEED). Since EXAFS can be thought of as a kind of spherical LEED with an electron gun and a phase-sensitive detector buried deep in a solid, it is natural to apply some of the knowledge gained in LEED studies to the present problem. In particular, several groups have calculated the phase shift of electrons scattered by atoms treated in the muffin-tin approximation. We will be using the program developed by Pendry⁶ in which the input are the core state wave functions obtained from Herman and Skillman.⁷ The conduction electrons are treated in one of two ways: (i) The Herman Skillman wave functions are truncated at the muffin-tin radius and the wave functions are normalized inside so that the correct number of conduction electrons per atom is obtained or (ii) the conduction electrons are simply represented by a uniform distribution of charge density within the muffin-tin sphere. While both of these approximations are crude by band-calculation standards, they should work reasonably well in the high-energy range of interest. In practice it is found that either method gives roughly the same phase shift. The important thing is to maintain the charge neutrality of the atom. The program by Pendry⁶ then calculates self-consistently within the Hartree-Fock approximation, the wave function and hence the phase shift of the electron being scattered including interaction with the atomic wave functions. Figure 4 shows some of the phase shifts for copper plotted as a function of electron wave number k expressed in atomic units ($\hbar = m = e = 1$). It is seen that the phase shifts are generally large (indeed by Levinson's theorem the $l = 0, 1, 2$ phase shifts must go through πn_l times, where n_l is the number of bound states with angular momentum l) and the Born approximation is not valid even at the highest energy. We also find that the number of phase shifts required to describe the scattering [using roughly the criterion $(2l + 1)\delta_l < 1$] increases with increasing energy and at 1000 eV we use 14 phase shifts. This is because a large l is required to describe the strong peaking in the forward direction of the scattering amplitude as the energy is increased. The scattering amplitude $f(\theta)$ is given by the formula

$$f(\theta) = \frac{1}{k} \sum_{l=0}^{\infty} (2l + 1) e^{i\delta_l} \sin\delta_l P_l(\cos\theta). \quad (2.1)$$

Plots of $|f(\theta)|$ for several energies are shown in Fig. 5.

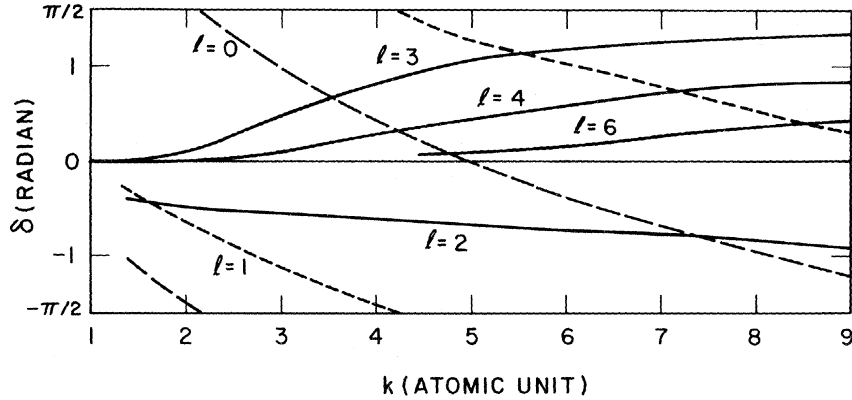


FIG. 4. Phase shift of electron scattering by copper atom for $l=1, 2, 3, 4, 6$ as a function of electron momentum k .

So much for scattering by the ion cores. The photoelectron also distorts the conduction and valence wave functions resulting in a correlation self-energy correction. Since the photoelectron can also excite plasma modes this self-energy has an imaginary component which reproduces the decay of the elastic (coherent) part of the photoelectron wave function. LEED studies⁶ have shown that the self-energy can be represented to a good approximation by a complex constant V_0 which for copper takes the value

$$V_{0r} = -15 \text{ eV}, \quad (2.2)$$

$$V_{0i} = -\eta_e = -4 \text{ eV}. \quad (2.3)$$

Both real and imaginary parts depend on the energy of the photoelectron but above the plasmon excitation threshold the energy dependence seems weak and we neglect it. We emphasize that it is only the inelastic scattering contribution that should be included in the damping of the photoelectron. Since we are basically dealing with interference phenomenon waves elastically scattered by other atoms should be viewed as multiple-scattering events which could enhance as well as reduce the wave functions arriving at a given atomic site. Such scattering will be treated in Sec. III. Here we only wish to stress that it is incorrect to approximate such multiple-scattering effects by an additional damping coefficient.

Our next step is to use the phase shifts to calculate the modification of the final state. The unperturbed final state is an outgoing spherical wave described by

$$\psi_0(\vec{r}) = \sum_{lm} A_{lm} h_l^{(1)}(kr) Y_{lm}(\Omega(\vec{r})). \quad (2.4)$$

We would like to describe the scattering of this wave by an atom located at \vec{R}_j . We first expand ψ_0 in spherical harmonics about \vec{R}_j using the following

expression which is valid for $|\vec{r} - \vec{R}_j| < |\vec{R}_j|$:

$$\psi_0(\vec{r}) = \sum_{l'm''} B_{l'm''} j_{l'}(k|\vec{r} - \vec{R}_j|) Y_{l'm''}(\Omega(\vec{r} - \vec{R}_j)), \quad (2.5)$$

where

$$B_{l'm''} = \sum_{lm} \sum_{l'm'} 4\pi i^{l-l'-l''} (-1)^{m'+m''} h_l^{(1)}(kR_j) \times Y_{l'-m'}(\Omega(\vec{R}_j)) \int Y_{lm} Y_{l'm'} Y_{l''-m''} d\Omega A_{lm}. \quad (2.6)$$

Equation (2.6) can be simplified by defining a matrix

$$[R^{lm}]_{l'm'',l'm'} = 4\pi i^{l-l'-l''} (-1)^{m'+m''} \times \int Y_{lm} Y_{l'm'} Y_{l''-m''} d\Omega \quad (2.7)$$

and a vector

$$v_{l'm''}(\vec{R}_j) = h_l^{(1)}(kR_j) Y_{l'm''}(\Omega(\vec{R}_j)). \quad (2.8)$$

Then the vector $B_{l'm''}$ is given by the matrix product

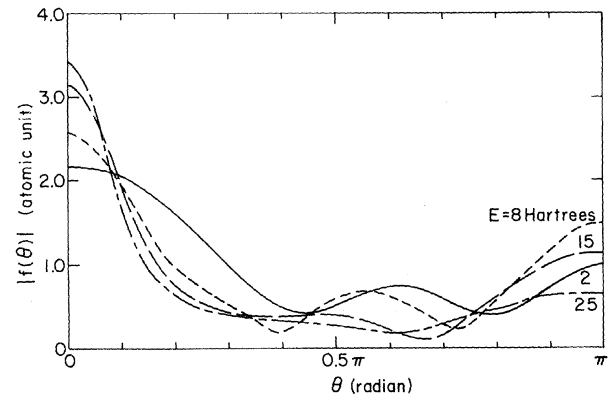


FIG. 5. Scattering amplitude $f(\theta)$ for energy $E=2, 8, 15, 25$ hartree (1 hartree = 27.2 eV).

$$B = \sum_{lm} R^{lm} v(\vec{R}_j) A_{lm}. \quad (2.9)$$

Note that the matrix R is independent of the atomic coordinates and can be computed once and for all.⁸

Once ψ_0 is expressed as spherical waves about the atom at \vec{R}_j , the scattered wave ψ_s^j emanating from \vec{R}_j is obtained simply in terms of the t matrix, which is in turn given by the phase shifts

$$\begin{aligned} \psi_s^j(\vec{r}) = & \sum_{LMi''m''} h_L^{(1)}(k|\vec{r}-\vec{R}_j|) Y_{LM}(\Omega(\vec{r}-\vec{R}_j)) \\ & \times T_{LM, i''m''} B_{i''m''}, \end{aligned} \quad (2.10)$$

where

$$T_{LM, i''m''} = \delta_{Li''} \delta_{Mm''} \frac{1}{2} (e^{2i\delta_L} - 1). \quad (2.11)$$

We note that the matrix T is related to the more standard t matrix by $t = iT/k$. Now $\psi_s^j(\vec{r})$ is an outgoing wave from the atomic position \vec{R}_j and can be expanded about the origin using Eq. (2.5) and (2.6) again,

$$\psi_s^j(\vec{r}) = \sum_{L''M''} C_{L''M''} 2j_{L''}(kr) Y_{L''M''}(\Omega(\vec{r})), \quad (2.12)$$

where we note that a factor of 2 has been introduced into the definition. This is because it is convenient to think of Eq. (2.12) as consisting of an incoming and an outgoing part and $2j_L = h_L^{(1)} + h_L^{(2)}$. The coefficient C_{LM} can be written in terms of R and v as defined in Eqs. (2.7) and (2.8). However, for computational purposes it is more convenient to group the indices in a slightly different way and introduce the matrix

$$\begin{aligned} [S^{L''M''}]_{L'M', LM} = & 2\pi i^{L-L'-L''} (-1)^{M'+M''} \\ & \times \int Y_{LM} Y_{L'M'} Y_{L''-M''} d\Omega. \end{aligned} \quad (2.13)$$

Then $C_{L''M''}$ is given by the matrix product

$$\chi(k) = \frac{2\text{Re} \left(\sum_{m_0} \sum_{im_0} P_{i_0 m_0, im} Z_{im, i'm'} P_{i'm', i_0 m_0} e^{i(\delta_i' + \delta_i'')} \right)}{\sum_{m_0} \sum_{im} |P_{i_0 m_0, im}|^2}, \quad (2.18)$$

where $P_{i_0 m_0, im}$ is the dipole matrix element between the core state $i_0 m_0$ and the conduction state with im symmetry. In Appendix A we indicate how Eq. (2.18) can be derived using a Green's-function expansion. It can also be obtained using the multiple-scattering formalism of Beeby⁹ and of Lloyd and Smith.¹⁰

For our numerical work we would like to specialize to the case of an s core level. For a cubic system it can be shown that $Z_{1m, 1m'}$ is diagonal. More generally for unpolarized x-rays we show in

$$\begin{aligned} C_{L''M''} = & v(-\vec{R}_j) S^{L''M''} T B \\ = & \sum_{im} v(-\vec{R}_j) S^{L''M''} T R^{lm} v(\vec{R}_j) A_{lm}. \end{aligned} \quad (2.14)$$

Finally summing over all atoms at $\vec{R}_j \neq 0$, we can write

$$C_{L''M''} = \sum_{im} Z_{L''M'', im} A_{im}, \quad (2.15)$$

where we have introduced the matrix Z ,

$$Z_{L''M'', im} = \sum_j v(-\vec{R}_j) S^{L''M''} T R^{lm} v(\vec{R}_j). \quad (2.16)$$

The matrix Z contains all the information we need to compute the EXAFS spectrum using the Golden Rule, Eq. (1.3). We can think of Eq. (2.16) for Z as the modification of the final state due to a single backscattering by each of the surrounding atoms. More generally we can think of a core electron in the state $i_0 m_0$ making a transition to an outgoing wave of quantum number $i' m'$ via the dipole matrix element $\langle i' m' | \vec{r} | i_0 m_0 \rangle$. The outgoing wave is scattered by the surrounding atoms resulting in an incoming wave with quantum number im about the original atom. The amplitude of this incoming wave is given by $Z_{im, i'm'}$. This incoming wave is coupled back to the core state by the matrix element $\langle i_0 m_0 | \vec{r} | i' m' \rangle$. Furthermore the photoelectron suffers a phase shift of $e^{i\delta_i'}$ on its outgoing trip and a factor of $e^{i\delta_i'}$ on its incoming trip. Adding the complex conjugate of the above process the adsorption rate is then given by

$$\begin{aligned} \frac{1}{\tau} = & \frac{2\pi}{\hbar} \left(\sum_{m_0} \langle i_0 m_0 | e^{\vec{\epsilon} \cdot \vec{r}} | im \rangle e^{i\delta_i'} Z_{im, i'm'} e^{i\delta_i''} \right. \\ & \left. \times \langle i' m' | e^{\vec{\epsilon} \cdot \vec{r}} | i_0 m_0 \rangle + \text{c. c.} \right) \delta(E_i + \hbar\omega - E_f). \end{aligned} \quad (2.17)$$

Dividing Eq. (2.17) by τ_0^{-1} we obtain

Appendix B that we should average over the diagonal elements of $Z_{im, i'm'}$, and Eq. (2.18) then simplifies to

$$\chi(k) = \frac{1}{3} \sum 2\text{Re}(Z_{im, im} e^{i2\delta_i}). \quad (2.19)$$

This is the equation we shall use and in the rest of the paper we shall concentrate on calculating the matrix Z . We find that Z can be given in terms of a multiple-scattering expansion [Eq. (A23)], the first term of which is the single-scattering contri-

bution given by Eq. (2.16).

To make contact with previous theory we shall make approximations in two steps.

(i) We assume that the atomic radius is small so that the curvature of the incident wave front can be neglected. Then instead of expanding the outgoing wave $Y_{lm} h_l^{(1)}(kr)$ about $\hat{\mathbf{R}}_j$ we can approximate it by a plane wave $\Phi_{\mathbf{F}}(\hat{\mathbf{r}})$ that has the same amplitude and phase at $\hat{\mathbf{R}}_j$. Noting that $h_l^{(1)}(kr)$ is of the form $P(kr)e^{ikr}$, where $P(kr)$ is a polynomial in $(kr)^{-1}$, we can write

$$\Phi_{\mathbf{F}}(\hat{\mathbf{r}}) = Y_{lm}(\hat{\mathbf{R}}_j) h_l^{(1)}(kR_j) e^{i\mathbf{k} \cdot (\hat{\mathbf{r}} - \hat{\mathbf{R}}_j)}, \quad (2.20)$$

where

$$\hat{\mathbf{k}} = k\hat{\mathbf{R}}_j \quad (2.21)$$

and $\hat{\mathbf{R}}_j$ is a unit vector in the $\hat{\mathbf{R}}_j$ direction. Using the expansion

$$e^{i\mathbf{k} \cdot \hat{\mathbf{r}}} = 4\pi \sum_{l'm'} i^l j_l(kr) Y_{l'm'}^*(\hat{\mathbf{k}}) Y_{l'm'}(\hat{\mathbf{r}}), \quad (2.22)$$

the scattered wave can easily be computed in the same way as in the derivation of Eq. (2.10) and we obtain

$$\begin{aligned} \Phi_s^j(\hat{\mathbf{r}}) &= \sum_{l'm'} h_l^{(1)}(k|\hat{\mathbf{r}} - \hat{\mathbf{R}}_j|) Y_{l'm'}(\Omega(\hat{\mathbf{r}} - \hat{\mathbf{R}}_j)) \\ &\quad \times \frac{1}{2} (e^{2i\delta_{l'}} - 1) 4\pi i^l Y_{lm}(\hat{\mathbf{R}}_j) Y_{l'm'}^*(\hat{\mathbf{R}}_j) h_l^{(1)}(kR_j). \end{aligned} \quad (2.23)$$

Again $\Phi_s^j(\hat{\mathbf{r}})$ can be approximated by a plane wave with the same amplitude and phase at the origin propagating in the direction $-\hat{\mathbf{R}}_j$,

$$\Phi_{-\hat{\mathbf{R}}_j}^j(\hat{\mathbf{r}}) = \Phi_s^j(\hat{\mathbf{r}}=0) e^{-i\mathbf{k} \cdot \hat{\mathbf{r}}}. \quad (2.24)$$

Using Eq. (2.22), $\Phi_{-\hat{\mathbf{R}}_j}^j(\hat{\mathbf{r}})$ is expanded as spherical harmonics and the coefficient of that expansion identified with the matrix Z :

$$\Phi_{-\hat{\mathbf{R}}_j}^j(\hat{\mathbf{r}}) = \sum_{l''m''} Z_{l''m'',lm}^j 2j_{l''}(kr) Y_{l''m''}(\hat{\mathbf{r}}). \quad (2.25)$$

After some simplification using the addition theorem for spherical harmonics we obtain

$$\begin{aligned} Z_{l''m'',lm}^j &= 2\pi i^{l''} Y_{l''m''}^*(-\hat{\mathbf{R}}_j) h_l^{(1)}(kR_j) \\ &\quad \times \sum_{l'} P_l(\cos\pi) \frac{1}{2} (e^{2i\delta_{l'}} - 1) h_{l'}^{(1)}(kR_j). \end{aligned} \quad (2.26)$$

This approximate form requires only a single l sum and is considerably simpler than the more accurate expression given by Eq. (2.16).

(ii) The next level of approximation we can make is that $kR_j \gg 1$ for all R_j . Then $h_l^{(1)}(kR_j)$ can be replaced by its asymptotic form

$$h_l^{(1)}(\rho) \xrightarrow{\rho \rightarrow \infty} -i\rho^{-1} e^{i(\rho - l\pi/2)} \quad (2.27)$$

The sum over l' is then precisely the form for the backscattering amplitude $f(\theta = \pi)$ and Eq. (2.26) simplifies to

$$\begin{aligned} Z_{l''m'',lm}^j &= -i2\pi i^{l''-l} Y_{l''m''}^*(-\hat{\mathbf{R}}_j) Y_{lm}(\hat{\mathbf{R}}_j) \\ &\quad \times \frac{e^{i2kR_j}}{kR_j^2} f(\pi). \end{aligned} \quad (2.28)$$

For s core states and unpolarized x rays we use Eq. (2.19) to obtain

$$\chi(k) = \sum_j \frac{N_j}{kR_j^2} \sin[2kR_j + 2\delta_l'(k) + \psi(k)] |f(\pi)| e^{-\gamma R_j}, \quad (2.29)$$

where we have written

$$f(\theta) = |f(\theta)| e^{i\psi}. \quad (2.30)$$

As discussed earlier we have included damping by adding a small imaginary part η to the photoelectron energy E . We have further expanded for small damping

$$k = [2(E + i\eta)]^{1/2} \approx (2E)^{1/2} + i\eta/(2E)^{1/2} \quad (2.31)$$

and identified γ as $\eta/(2E)^{1/2}$. A Debye-Waller factor can be introduced as being due to thermal smearing of the atomic position. Comparison with Eq. (2.4) indicates that our approximate form is in substantial agreement with the result of Sayers *et al.*, apart from an additional phase factor from the scattering amplitude. We have also introduced an energy-dependent decay factor. In our numerical work for copper we have used $\eta = 4$ eV, which is a number obtained from LEED experiment.

In order to examine the effect of these approximations we have calculated on a computer the unapproximated expression for Z given by Eq. (2.16). Since we expect Z to be oscillatory we have defined

$$\tilde{Z}^j = e^{-i2kR_j} \frac{1}{3} \sum_m Z_{lm,lm}, \quad (2.32)$$

which is a smooth function of k . For the purpose of illustration we show in Figs. 6 and 7 the amplitude $|\tilde{Z}|$ and phase $\tilde{\phi}$ for \tilde{Z} for the first and third shells. Also shown in Fig. 6 is $|\tilde{Z}|$ calculated using the approximate expression given by Eq. (2.26). It can be seen that the approximate expression works very well for the amplitude $k > 3$ or $E > 100$ eV. The next level of approximation in terms of the scattering amplitude, i.e., Eq. (2.29), essentially agrees with Eq. (2.26) over the entire range and has not been plotted. In Fig. 7 we show the phase $\tilde{\phi}$ calculated using all three expressions. The dotted line is that given by Eq. (2.29) and is of course independent of shell radius. It differs substantially from the spherical-wave expression and the plane-wave approximation given

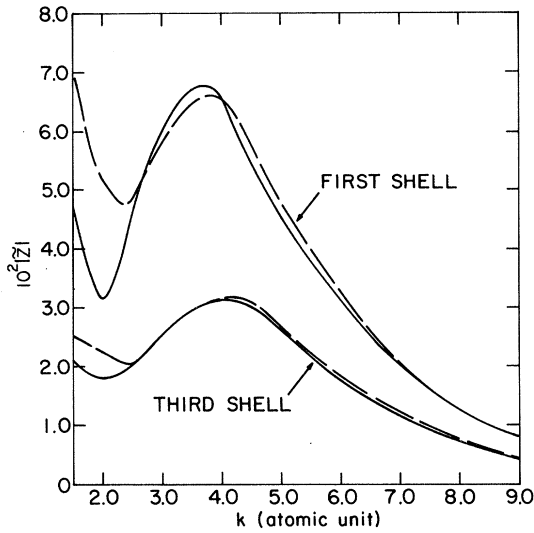


FIG. 6. Amplitude of the function \tilde{Z} [from which the EXAFS oscillation can be obtained using Eq. (2.35)] for the scattering of the photoelectron by the first and the third shell. Solid lines are the spherical-wave theory computed using Eq. (2.16) and dashed lines are the small-atom approximation using Eq. (2.26).

by Eq. (2.24) lies somewhere in between. We see that in the present situation where $kR \geq 5$ there remains a sizable difference between the last two approximate forms for the phase θ even though they agree for the amplitude $|\tilde{Z}|$. Furthermore, both of these approximations differ considerably from the spherical-wave expression. In particular, even though the plane-wave approximation shows some difference between the two shells, the difference is not nearly as dramatic as that given by the more accurate expression. This is because the spherical-wave expression takes into account the finite size of the atom. If we take the crude model that $f(\pi)$ is the radius of the region of the atomic potential which contributes to the backscattering, then the plane-wave wave front has a phase difference at the edge of this region from the spherical-wave wave front given by

$$\delta\Phi = k[f(\pi)]^2/R_j. \quad (2.33)$$

The criterion for the validity of the plane-wave or small-atom approximation is then that $\delta\Phi \ll 1$. The expression given by Eq. (2.33) is not too small at low energy and decreases only gradually for large k . Thus for the relatively small values of R_j we are studying the small-atom approximation is accurate only at relatively high energy. However, the main correction for backscattering appears to be in the phase and not the amplitude.

The amplitude $|\tilde{Z}|$ shows a broad maximum around $k=4$ or $E \sim 200$ eV. This agrees quite well with the experimentally observed peaking of the

EXAFS oscillations around the same energy. Furthermore while the phase $\tilde{\Phi}$ shows quite a variation over the entire energy range, it is relatively slowly varying in the region when $|\tilde{Z}|$ is at a maximum. This may indicate that at least for copper the k dependence in the phase of \tilde{Z} is dominated by the central-atom phase shift. Whether this is true for other elements remains to be investigated.

We next compute the central-atom phase shift δ'_1 . This is done by removing one electron from the $1s$ core state and spreading the charge uniformly within the Wigner-Seitz sphere. This is a very crude description of a screened excited atom and is probably the most unreliable portion of this work. The result of the computation is shown in Fig. 8 and we can see that it is remarkably linear in k . In the range $k=3$ to 5 we have approximately $\delta'_1 \approx -0.4k$. This implies a shift of the radial distances determined from EXAFS from the true distances by roughly 0.4 a. u., or 0.2 \AA . The experimentally observed shift is more like 0.34 \AA .

It is straightforward to obtain from \tilde{Z} the EXAFS oscillation $\chi(k)$ using Eqs. (2.19) and (2.32),

$$\chi(k) = \sum_j 2|\tilde{Z}_j| \cos(2k\gamma_j + \tilde{\Phi}_j + 2\delta'_1). \quad (2.34)$$

The result is plotted vs electron energy in Fig. 9(c). We have included a Debye-Waller factor¹¹ with $2\sigma^2 = 0.022$ for comparison with experiment performed at 77° . The experimental $\chi(E)$ is shown in Fig. 9(a). The first five prominent peaks occur at the following theoretical (experimental) values in eV: 57 (47); 105 (95); 172 (157); 218 (201); 250 (235). The choice of an E_0 of 15 eV

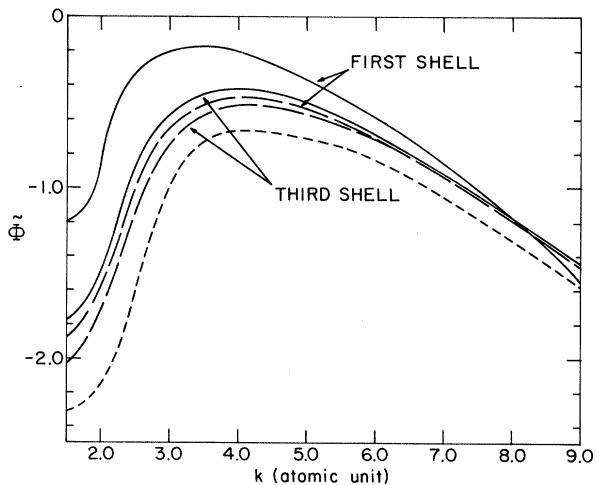


FIG. 7. Phase $\tilde{\Phi}$ of the function \tilde{Z} for the first and third shell. Solid lines refer to the spherical-wave theory [Eq. (2.16)], long-dashed lines refer to the small-atom approximation [Eq. (2.26)], and short-dashed line is the large- kR limit [Eq. (2.29)] which is independent of shell radii.

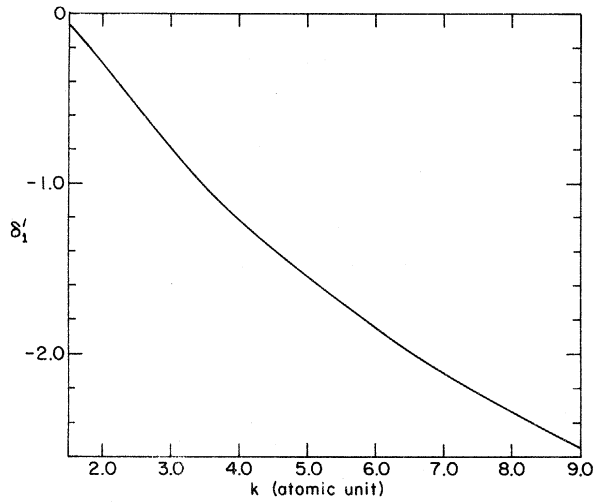


FIG. 8. $l=1$ phase shift in radians for the screened excited central atom.

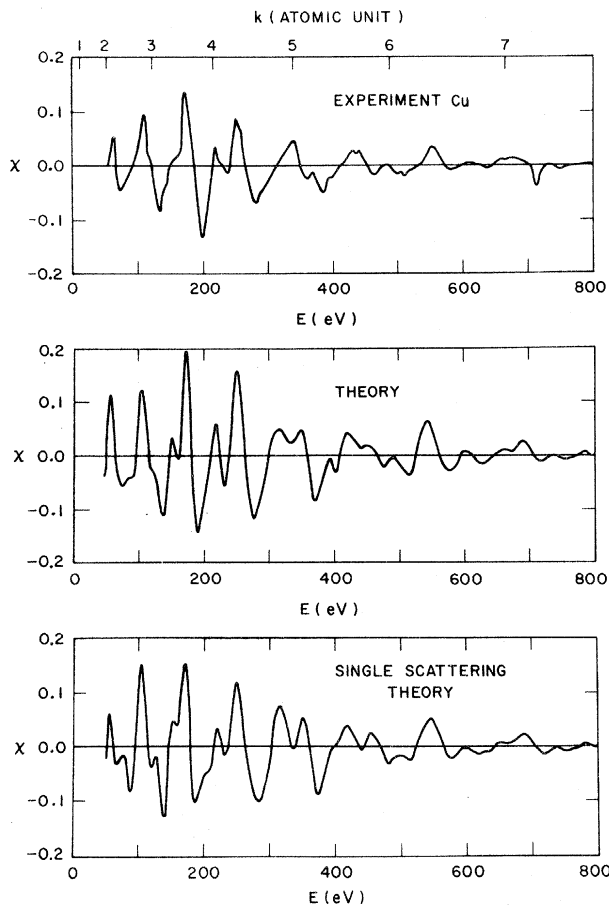


FIG. 9. EXAFS oscillation χ plotted vs photoelectron energy. (a) Experimental curve. The energy has been measured from the threshold plus a correction of 15 eV. (b) Theoretical curve including multiple-scattering effects. (c) Theoretical curve including single backscattering from surrounding atoms only.

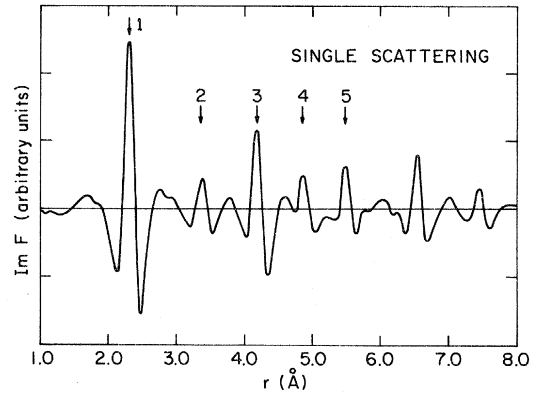


FIG. 10. Imaginary part of the Fourier transform of $\chi(k)$ including single scattering only.

matches the last three peaks rather nicely and we have shifted the experimental plot by this amount. The relatively large shift and the fact that it depends on the photoelectron energy is a consequence of our uncertainty about the central-atom phase shift and also uncertainty in the experimentally defined threshold. The absolute value of $\chi(E)$ and the shape of the envelope compares quite favorably with the experimental observation. The situation improves somewhat when we include multiple scattering in Sec. III, the result of which is shown in Fig. 9 (b).

We next perform the Fourier transform.

$$F(r) = \int \frac{dk}{2\pi} e^{-i2kr} \chi(k). \quad (2.35)$$

Owing to our uncertainty concerning the lower energy range the k integration begins at $k=1.9$. A similar cutoff has been used by the experimentalists. We have performed the Fourier-transform calculation at zero temperature; i.e., we have removed the Debye-Waller factor from $\chi(k)$. For the single-scattering contribution the Debye-Waller factor simply changes the absolute magnitude of $F(r)$. Multiple-scattering effects, however, are reduced relative to the single scattering peaks by temperature. In Fig. 10 we show the imaginary part of $F(r)$. (The real part looks very similar except for a shift in phase.) It clearly shows peaks at the shell distances but shifted uniformly downward by approximately 0.24 \AA . As we would expect the shells are all in phase with each other and Fig. 10 does not show the inversion in the fourth shell that is observed experimentally. Thus while the single-scattering theory can account for various qualitative features of EXAFS, some serious difficulties remain. In order to explain the discrepancy we will need to include multiple-scattering effects.

III. MULTIPLE SCATTERING

In Sec. II we have included corrections to the final state by considering only backscattering from neighboring atoms. Clearly there are additional corrections if the electron is scattered by several atoms before returning to the central atom. Whereas the amplitude of the scattered wave becomes smaller the number of possible paths increases and it is not obvious that such multiple-scattering effects are small. Indeed in the case of LEED it is known that it is important to take into account multiple scattering to all orders to get agreement with experiment. Typically this is done by constructing the scattering matrix for each atomic layer and then adding up all possible propagation from layer to layer.^{6,12} In the case of EXAFS the planar geometry is replaced by a spherical one. An analogous procedure would be to compute the scattering matrix for each shell in terms of a spherical-wave expansion. However, unlike the planar case the symmetry of the atomic position within each shell differs significantly from shell to shell. Such a procedure will be rather cumbersome and in practice will probably be limited to a few shells. Ashley and Doniach¹³ have carried out calculations in which they included the effect of multiple scattering exactly for the first two shells. The scattering has been assumed to be *s* wave only. In view of the increasing importance of higher-order phase shifts at increasing energy, their calculation is probably limited in applicability to relatively low energy, ≤ 100 eV. Since the EXAFS spectrum peaks around 200 eV we are more interested in the effect of multiple scattering at energy ≥ 50 eV. In this sense our approach is complementary to that of Ashley and Doniach.

Another possible approach for including multiple-scattering effects, at least for crystalline materials, is to calculate the band structure. Except for the excited atom at the origin the crystal still has translational symmetry and it should be possible to construct Bloch wave solutions which include all multiple-scattering effects and treat the central atom as a perturbation in the end. This line of reasoning is quite similar to that of Kronig,¹⁴ who argued that EXAFS can be understood from the position of the band gaps. The difficulty with this approach has been analyzed recently by Stern.¹⁵ As he pointed out it is clear from Eq. (2.1) that EXAFS comes from modification of the final state and in terms of a band calculation it is a matrix-element effect. Such effects are linear in the pseudopotential Δ whereas corrections due to the existence of band gaps, i. e., density-of-states effects, are second order in Δ . The reason is that while the band gap is of order Δ , the region

in k space in which it is an important correction is also linear in Δ . Thus density-of-states corrections constitute a higher-order effect. Hence in an energy-band-type calculation one will have to focus one's attention on matrix-element effects. As we will see this is in a sense what we are trying to accomplish.

From the above discussion it is clear that a calculation that includes all multiple-scattering effects will be very difficult. However, in the present problem there is one important simplifying factor. Since we are ultimately interested in Fourier transforming the absorption coefficient to obtain oscillations in position space, at a given radial distance we can ask ourselves what are the multiple-scattering effects that will contribute to the Fourier transform at that particular radius. This leads us to classify the multiple-scattering contribution in terms of path length. If the electron propagates from the origin to an atom at \vec{R}_1 , where it is scattered and propagated to an atom at \vec{R}_2 , where it is scattered back to the origin, one expects the modification of the final state will be proportional to

$$\chi(k) \propto f(\theta_1)f(\theta_2)e^{ikR_1}e^{ik|\vec{R}_1-\vec{R}_2|}e^{ikR_2}, \quad (3.1)$$

where $f(\theta)$ is the scattering amplitude and θ_1 , θ_2 are the scattering angles. By comparison with the single-scattering formula, Eq. (2.2), we see that we can define an effective radius

$$r_{\text{eff}} = \frac{1}{2}(R_1 + |\vec{R}_1 - \vec{R}_2| + R_2) \quad (3.2)$$

for each multiple-scattering path and the Fourier transform of its contribution to the absorption coefficient will peak at r_{eff} . Provided that its transform is not too spread out in r space we need to consider only a finite number of paths if we are interested in the structure within a finite radius around the central atom. This procedure is a convergent one in the sense that the "tail" from paths with large r_{eff} will not add up to give a large contribution at a given radius. This is because we have an exponential damping term that goes like $e^{-\gamma r_{\text{eff}}}$ multiplying each contribution.

In Table I we list all the possible paths up to the fifth-shell radius together with the number of independent paths for each r_{eff} . We use the label 1-3-1 to indicate a path which goes from the origin to atom *A*, which is on the first shell, and then to another first-shell atom, *B*, where the distance between *A* and *B* is that corresponding to a third shell. We then have $r_{\text{eff}} = \frac{1}{2}(R_1 + R_3 + R_1)$, where R_1 and R_3 are the distances to the first and third shells, respectively. For a given r_{eff} there may of course be more than one type of scattering corresponding to the different orders in which the electron is scattered by the neighboring atoms. One has to be careful to add up all these contribu-

TABLE I. Characterization of shell radius and effective shell radius for copper in the fcc lattice.

Shell	Radius (r_{eff}) (Å)	No. of paths
1	2.55	12
2	3.61	6
1-1-1	3.83	48
1-2-1	4.36	72
3	4.43	24
1-3-1	4.77	144
4	5.11	12
1-1-4	5.11	36
1-1-1-1	5.11	
1-2-3	5.30	144
1-3-3	5.61	144
5	5.72	24

tions. We note here that for the distances considered we can restrict ourselves to double scattering with the exception of the 1-4-1 paths, which will be discussed later.

It is a straightforward matter to extend the single-scattering calculation presented in Sec. III, to include multiple scattering. We simply expand the outgoing wave after it has been scattered by the first atom about the second atoms and then reexpand the scattered wave about the origin. The only difficulty is that the size of the matrices goes up rapidly as the number of phase shifts increases and for our numerical work we are restricted to a maximum of seven phase shifts. This is clearly inadequate at high energy and we will return to this point later. The formalism for multiple scattering and the appropriate expansion is given in Appendix A. The result can be summarized as a correction to the matrix Z . Adopting the shorthand notation that L is equivalent to l , m we obtain from Eqs. (A23) and (A24)

$$Z_{LL'}^{\text{tot}} = \sum_{j \neq 0} Z_{LL'}^j + \sum_{j \neq k \neq 0} Z_{LL'}^{kj} + \dots, \quad (3.3)$$

where $Z^{i \dots kj}$ describe the scattering of the photoelectron by atoms at \vec{R}_j , \vec{R}_k , and finally \vec{R}_i . Its propagation is described by the matrix K and the expansion about the original atom by the matrix Q as follows:

$$Z^{i \dots kj} = Q(\vec{R}_i) T K(\vec{R}_i - \vec{R}_k) T \dots T K(\vec{R}_j), \quad (3.4)$$

where

$$K_{LL'}(\vec{R}) = \sum_{L_1} R_{L'L_1}^L v_{L_1}(\vec{R}), \quad (3.5)$$

$$Q_{LL'}(\vec{R}) = \sum_{L_1} v_{L_1}(-\vec{R}) S_{L'L_1}^L, \quad (3.6)$$

and v , R , S , and T have been defined in Sec. II.

It is also straightforward to generalize the

small-atom approximation as discussed in Sec. II. Again we replace the wave front at each atom by a plane wave. We obtain the following:

(i) Plane-wave approximation:

$$Z_{lm, l'm'} = g(-\vec{R}_k, \vec{R}_k - \vec{R}_j) g(\vec{R}_k - \vec{R}_j, \vec{R}_j) \\ \times 2\pi (-i)^l Y_{lm}^*(\hat{R}_k) Y_{l'm'}(\hat{R}_j) h_l^{(1)}(kR_j),$$

where (3.7)

$$g(\vec{R}_2, \vec{R}_1) = \sum_l (2l+1) P_l(\cos \theta) i^{l+\frac{1}{2}} (e^{2i\phi_l} - 1) h_l^{(1)}(kR_2), \quad (3.8)$$

where θ is the angle between \vec{R}_1 and \vec{R}_2 . Equations (3.7) and (3.8) have the advantage that only one sum over l' is required. Hence the computation is straightforward and one could include as many phase shifts as is necessary.

(ii) We can next take the limit $kR_j \gg 1$. The function g then becomes proportional to the scattering amplitude $f(\theta)$ and we have

$$Z_{lm, l'm'}^{kj} = f(\theta_2) f(\theta_1) 2\pi i (-i)^{l+l'} Y_{lm}^*(\hat{R}_k) Y_{l'm'}(\hat{R}_j) \\ \times \frac{e^{i k(R_j + |\vec{R}_k - \vec{R}_j| + \vec{R}_j)}}{k R_j R_k |\vec{R}_j - \vec{R}_k|}, \quad (3.9)$$

where θ_1 is the angle between \vec{R}_j and $\vec{R}_k - \vec{R}_j$, and θ_2 that between $\vec{R}_k - \vec{R}_j$ and $-\vec{R}_k$. Equation (3.9) corresponds to what we obtained based on intuitive arguments in Eq. (3.1).

In the case of unpolarized x-ray source and polycrystalline samples all the relevant information is contained in \tilde{Z} defined in analogy with Eq. (2.32). For each r_{eff} we have

$$\tilde{Z}(r_{\text{eff}}) = e^{-i2kr_{\text{eff}}} \frac{1}{3} \sum_{\text{path}} \sum_m Z_{lm, lm}, \quad (3.10)$$

where the first sum is over all paths with the same r_{eff} . In Figs. 11 and 12 we show the amplitude and phase of \tilde{Z} for various r_{eff} calculated using Eqs. (3.3) and (3.4), including seven phase shifts. Except for the 1-4-1 case we see that multiple-scattering effects generally have a peak value of 1%. This is much smaller than the contribution of single scattering from the first and third shell for instance, but quite comparable to some of the weaker shells. On the other hand, the multiple-scattering contribution is somewhat more rapidly varying in k space and hence tends to spread out more in r space. Over all, we find for copper that they contribute to a quantitative change in the Fourier transform, but do not affect the single-scattering peaks sufficiently severely to give qualitative change. The exception is the 1-1-4 path. In fcc structure the fourth shell consists of the 12 atoms at the corner of the faces; i. e., when viewed from the central atom they are shadowed by the first-shell atoms. The outgoing wave reach-

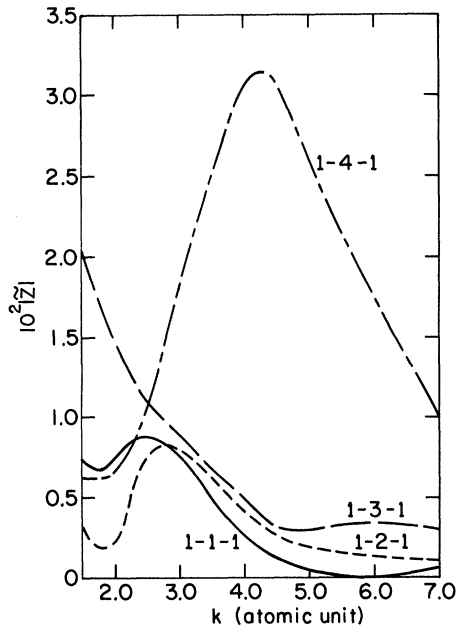


FIG. 11. Absolute value of Z for several paths using the spherical-wave theory Eq. (3.4).

ing the fourth shell will clearly be strongly affected by forward scattering due to the first-shell atoms. We see from Fig. 5 that the forward-scattering amplitude increases with energy and is quite large

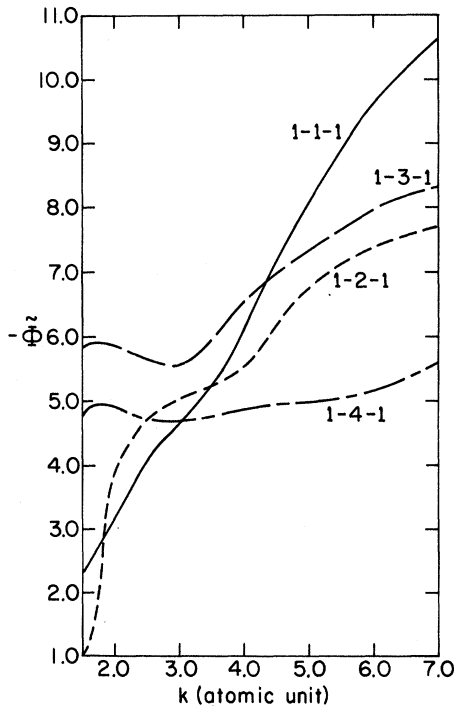


FIG. 12. Phase $\tilde{\phi}$ of \bar{Z} for several paths using Eq. (3.4).

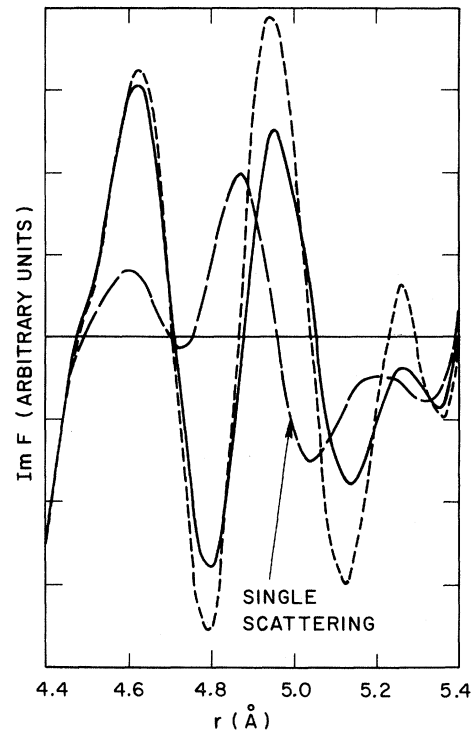


FIG. 13. Imaginary part of the Fourier transform of $\chi(k)$ in the region near the fourth-shell radius. The long-dashed line includes single scattering only while the solid line includes multiple scattering. The short-dashed line is a calculation in which the forward scattering by the first shell is calculated in the small-atom approximation. This approximation enables us to include more phase shift and is probably a better description of the forward scattering.

in magnitude. In fact, at the fourth shell the amplitude of the scattered wave due to the first shell can be larger than that of the unscattered wave. In this particular case multiple scattering will affect the results qualitatively. This can be seen from the large magnitude of $|\bar{Z}|$ shown in Fig. 11. Since the forward-scattering amplitude is so large, in our calculations we have also included the possibility of the electron being scattered in both its outgoing and incoming trips. We have neglected, however, other triple scattering of the same r_{eff} , i. e., when the electron bounces around three atoms all in the first shell. These are finite-angle scattering and are expected to be small. Multiple-scattering effects then dominate over the single-scattering contribution of the fourth shell. In particular, forward scattering introduces additional phase shifts and in the Fourier transform the fourth shell can be expected to behave quite differently from the other shells. In Fig. 13 we show the Fourier transform $\text{Im}F(r)$ in an expanded scale around the fourth shell, com-

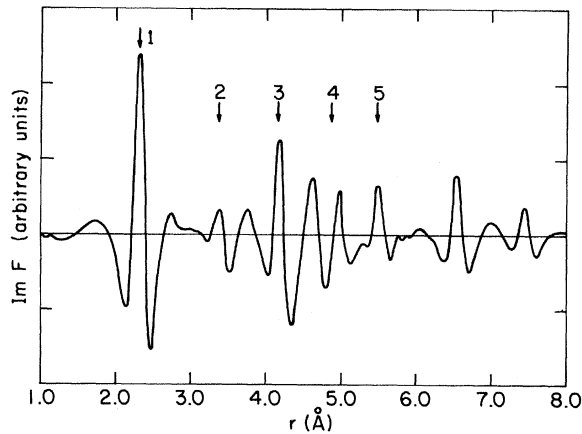


FIG. 14. Imaginary part of the Fourier transform of $\chi(k)$ including the effects of multiple scattering.

paring the contribution from single backscattering with the result of including multiple scattering. We find that the fourth shell has suffered approximately a 90° phase shift. This phase shift can be understood as arising from the difference between the phase ϕ for the 1-1-4 path as shown in Fig. 12 from that for the fourth shell by single scattering alone.

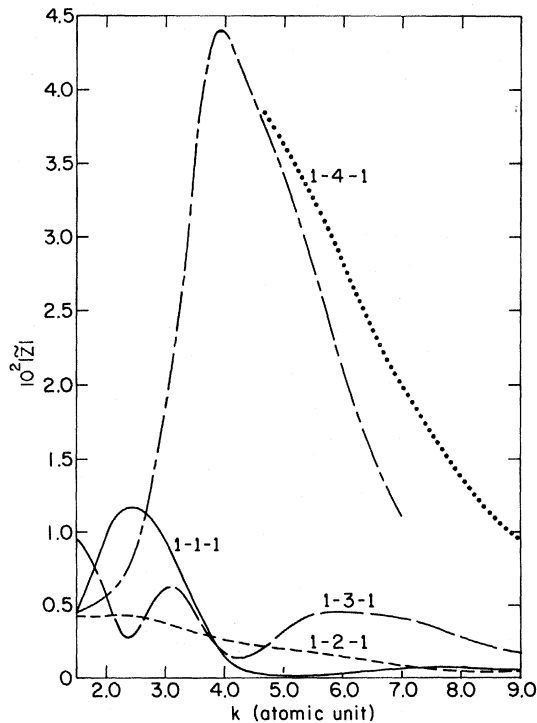


FIG. 15. Absolute value of \tilde{Z} for several paths using the small-atom approximation [Eq. (3.7)]. For the 1-4-1 path the dash-dot line includes seven shifts while the dotted line includes 14. The other paths are not as sensitive to the number of phase shifts.

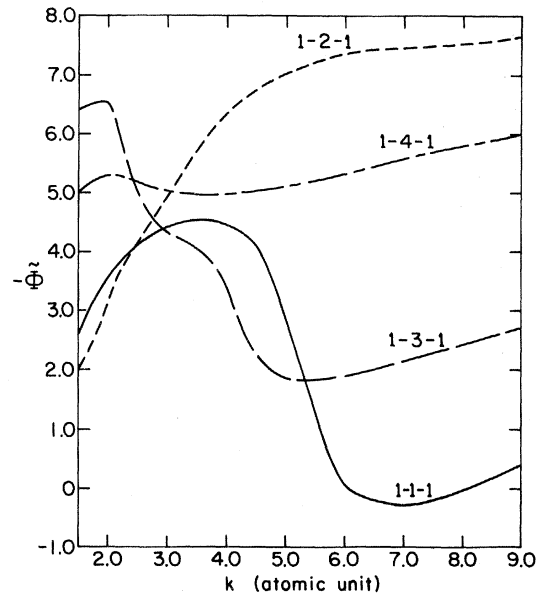


FIG. 16. Phase $\tilde{\phi}$ of \tilde{Z} calculated using the small-atom approximation.

In Fig. 14 we show the Fourier transform including multiple-scattering effects. As mentioned earlier one can see quantitative difference between this and the single-scattering curve but the most striking change is in the fourth shell. Whereas the experiment indicated a phase shift that is closer to 180° for the fourth shell, qualitatively we believe that multiple scattering accounts for the anomalous behavior near the fourth shell. We should also point out that our calculation is an underestimation of the effect of forward scattering because we have kept only seven phase shifts which we know to be inadequate to describe forward scattering in the energy range of interest.

We have also performed the calculation using the approximate expression given by Eqs. (3.7) and (3.8). Such calculations are very simple and can provide one with a qualitative understanding of the situation. Furthermore, only one sum over l is required and one can include as many phase shifts as one pleases. This provides us with a feeling as to when it is important to keep a large number of phase shifts. The resulting amplitude and phase for \tilde{Z} are shown in Figs. 15 and 16. We see that the 1-4-1 path agrees fairly well in both amplitude and phase with the more accurate spherical-wave calculation. Furthermore we find that when we include 14 phase shifts instead of seven the amplitude increases substantially, especially in the high- k range. This verifies our earlier statement that our calculation is an underestimation of the effect. For completeness we have used the approximate $|\tilde{Z}|$ for the fourth shell to calculate $F(r)$. The result is shown in Fig. 13. We see

that the "inversion" of the fourth peak is more pronounced and the result compares more favorably with experiment. On the other hand, for the other paths the approximate formula does not do so well, particularly in view of the success we had for the single-scattering case shown earlier in Fig. 6. There we found that for backscattering the small-atom approximation overestimates $|\tilde{Z}|$ at small k . The reason is that in the backward directions $f(\theta)$ is at a local maximum. Since the spherical-wave theory takes into account the finite size of the atoms, in a crude sense we can argue that this is analogous to some averaging of $f(\theta)$ near 180° and hence gives rise to a smaller result. On the other hand the multiple-scattering paths such as 1-1-3 involve finite scattering angle, where $f(\theta)$ may be near a local minimum. In such cases the plane-wave approximation will underestimate the result. Furthermore, a minimum of $f(\theta)$ means that there is large cancellation between contributions from different angular momenta in the sum given by Eq. (2.1). Hence the approximate treatment of the partial waves done in the small-atom approximation may lead to a rather inaccurate answer. Of course the error is compounded as the number of scatterings increases. Thus we see that the small-atom approximation approaches that of the spherical-wave theory only for a relatively large value of $k \gtrsim 5$. For forward scattering, however, contributions from various partial waves add and the small-atom approximation works relatively well. We should also mention that the small-atom approximation indicates that paths apart from 1-1-4 are not too sensitive to the number of phase shifts included beyond the first six or seven. Apparently a large number of phase shifts are required to describe the strong peaking of the scattering amplitude in the forward direction, whereas in the other directions they are not as crucial.

The phase of \tilde{Z} shown in Fig. 16 for the small-atom approximation appears to be very different from that in Fig. 12, with the exception of the 1-1-4 path. This is not as disturbing as it first appears because $\tilde{\phi}$ is defined only modulo 2π and the region of rapidly varying $\tilde{\phi}$ coincides with the region of

small $|\tilde{Z}|$. Thus we can conclude that the small-atom approximation is a reasonably good approximation for $k \gtrsim 5$, and that except for forward scattering, a description in terms of seven phase shifts is probably adequate for all k . For future applications, a hybrid scheme, whereby one treats the high-energy forward scattering by Eqs. (3.7) and (3.8) and the other scattering paths by Eqs. (3.3) and (3.4) using six or seven phase shifts, should provide an accurate description of the situation.

IV. CONCLUSION

We have performed a calculation of the x-ray absorption coefficient and its Fourier transform $F(r)$ starting from atomic scattering phase shifts obtained from the Herman-Skillman wave functions. We relax the small-atom approximation made in previous treatments of EXAFS and include multiple-scattering effects. We also calculated the central-atom phase shift by assuming a screened ionized atom. The result is found to be a remarkably linear function of k , an assumption which is central to the theory of Sayers *et al.*² To compare with experiment we list in Table II the theoretical and experimental peak positions in $\text{Im}F(r)$. On comparison with the known crystallographic distances we obtained an average shift of -0.24 \AA from the theory vs -0.34 \AA from the experiment. The fourth shell cannot be analyzed in terms of such shifts and in fact in the experiment appears to be 180° out of phase from the predicted position. We can account for this difficulty qualitatively by showing that shadowing of the fourth shell by the first-shell atom introduces a large multiple-scattering correction. We would also like to point out that for the bcc structure the fourth shell is shadowed by the first shell in exactly the same way and hence is expected to show large phase shifts. This has been verified for iron and other bcc metals. The experimental situation for hcp metals is inconclusive because the shell structure is very complicated for an hcp structure with c/a ratio that does not correspond to perfect close packing. We believe that the shadowing effect explains the observed difference between the EXAFS structure of metals and semiconductors. In the diamond structure the first shell that is shadowed is the eighth shell, which is beyond the present experimental resolution. Furthermore, in this case the eighth shell radius is three times that of the nearest-neighbor spacing. Owing to the $1/r$ decay of the scattered wave the forward-scattering effect is not expected to dominate over the single-scattering path. On the other hand, the diamond structure is considerably more open and multiple scattering may contribute to additional observable structures in between known shell distances. Such a possibility is currently be-

TABLE II. Comparison of the theoretical shift in shell radius, α_{th} , with the experimental value, α_{expt} .

Shell	R_j (\AA)	R_{th}	$\alpha_{\text{th}} = R_{\text{th}} - R_j$	α_{expt}
1	2.55	2.31	-0.24	-0.34
2	3.61	3.36	-0.25	-0.37
3	4.43	4.18	-0.25	-0.32
4 ^a	5.11	4.79	-0.32	-0.35
5	5.72	5.49	-0.23	-0.31

^aFor the fourth shell the distances refer to the inverted peak.

ing explored.

In conclusion, we believe that multiple-scattering effects in EXAFS can be understood in a fairly straightforward manner. Except for the shadowing effect we discussed the effect of multiple scattering is generally smaller than the major structure due to single scattering. With care and experience it should be possible to extract information on shell radii from these single-scattering peaks.

ACKNOWLEDGMENTS

We are thankful to T. M. Rice for many helpful ideas in the initial stage of the work. One of us (P. A. L.) is particularly thankful to D. E. Sayers and E. A. Stern for encouragement and discussions of the experimental situation. We also thank S. Doniach and P. Eisenberger for helpful discussions.

APPENDIX A

In this appendix we outline a calculation of the x-ray absorption coefficient η using Green's-function technique. We will obtain the result in the form of a multiple-scattering expansion corresponding to scattering of the excited electrons by the neighboring atoms. The absorption coefficient η is given by

$$\eta = (\omega/c)\epsilon''(\omega), \quad (\text{A1})$$

where ϵ'' is given in the dipole approximation as

$$\epsilon''(\omega) = 4\pi e^2 \text{Im} \left(\int \frac{d\nu}{2\pi} \int d\vec{r} d\vec{r}' i(\vec{\epsilon} \cdot \vec{r})(\vec{\epsilon} \cdot \vec{r}') \right. \\ \left. \times G(\vec{r}, \vec{r}', \nu) G_{\text{core}}(\vec{r}', \vec{r}, \nu - \omega) \right) \quad (\text{A2})$$

and $\vec{\epsilon}$ is the polarization vector of the x-ray electric field. The core-state Green's function is given in terms of the core wave function $\phi_{L_0}(\vec{r})$ with angular momentum $L_0 (= l_0, m_0)$ and binding energy ϵ_c and lifetime η_c^{-1} ,

$$G_{\text{core}}(\vec{r}', \vec{r}, \nu) = \frac{\phi_{L_0}(\vec{r}')\phi_{L_0}(\vec{r})}{\nu - \epsilon_c - i\eta_c}. \quad (\text{A3})$$

The Green's function $G(r, r', \nu)$ in Eq. (A2) is that for the excited electron moving in the muffin-tin potentials $\sum_i v_i(\vec{r} - \vec{R}_i)$ of the atoms. In our model all the atoms except the central excited atom are described by the same potential. The Green's function can be expanded in terms of the free electron $G_0(r, r')$ as

$$G(\vec{r}, \vec{r}') = G_0(\vec{r}, \vec{r}') T(\vec{r}_1, \vec{r}_2) G_0(\vec{r}_2, \vec{r}'). \quad (\text{A4})$$

Here we have adopted a notation that repeated indices are to be integrated over. It has been shown⁹ that T can be expressed as a series expansion in terms of $t(\vec{r}, \vec{r}')$, which is the t matrix for scatter-

ing by a single muffin-tin potential:

$$T(\vec{r}, \vec{r}') = \sum_j t_j(\vec{r} - \vec{R}_j, \vec{r}' - \vec{R}_j) \\ + \sum_{i \neq j} t_i(\vec{r} - \vec{R}_i, \vec{r}_1 - \vec{R}_i) G_0(\vec{r}_1 - \vec{r}_2) \\ \times t_j(\vec{r}_2 - \vec{R}_j, \vec{r}' - \vec{R}_j) + \dots, \quad (\text{A5})$$

where

$$t(\vec{r}, \vec{r}') = v(\vec{r})\delta(\vec{r} - \vec{r}') + v(\vec{r})G_0(\vec{r} - \vec{r}')v(\vec{r}') \\ + v(\vec{r})G_0(\vec{r} - \vec{r}_1)v(\vec{r}_1)G_0(\vec{r}_1, \vec{r}')v(\vec{r}') + \dots \quad (\text{A6})$$

Equation (A5) can be interpreted as multiple scattering of the electron by successive atoms and the sum is under the restriction that there should be no successive scatterings by the same atom.

For the present problem we are interested in $G(\vec{r}, \vec{r}', \nu)$ where \vec{r} and \vec{r}' are within the central-atom muffin tin. This is because the core wave function in Eq. (A3) is highly localized. Furthermore, we assume that the central photoexcited atom can be represented by a different potential v_0 and a t matrix t_0 . Then it is convenient to solve the scattering problem of the electron by the central atom exactly and introduce the Green's function G_c ,

$$G_c(\vec{r}, \vec{r}') = G_0(\vec{r}, \vec{r}') + G_0(\vec{r}, \vec{r}_1)t_0(\vec{r}_1)G_0(\vec{r}_1, \vec{r}'). \quad (\text{A7})$$

For \vec{r}, \vec{r}' inside the muffin-tin radius r_{MT} , we have

$$G(\vec{r}, \vec{r}') = G_c(\vec{r}, \vec{r}') + \sum_j' G_c(\vec{r}, \vec{r}_1)t(\vec{r}_1 - \vec{R}_j, \vec{r}_2 - \vec{R}_j) \\ \times G_c(\vec{r}_2, \vec{r}') + \sum_{i \neq j} G_c(\vec{r}, \vec{r}_1)t(\vec{r}_1 - \vec{R}_j, \vec{r}_2 - \vec{R}_i) \\ \times G_0(\vec{r}_2 - \vec{r}_3)t(\vec{r}_3 - \vec{R}_j, \vec{r}_4 - \vec{R}_j)G_c(\vec{r}_4 - \vec{r}') + \dots, \quad (\text{A8})$$

where the sum is further restricted so that the first and last t matrix should not refer to the central atom. The Green's function G_c can be constructed from the solution of the muffin-tin potential v_0 , which is most conveniently obtained by a spherical-harmonics expansion. Including only states above the Fermi surface, we obtain

$$G_c(\vec{r}, \vec{r}', \nu) = \sum_{L', R} \frac{\phi_{L', R}(\vec{r})\phi_{L', R}^*(\vec{r}')}{\nu - \epsilon_{L', R} + i\eta_e}, \quad (\text{A9})$$

where

$$\phi_{L',k}(r) = \begin{cases} (2\pi/R)^{1/2} \phi_{L',k}^0(r), & r < r_{MT} \\ (1/2R)^{1/2} k i^{l'} Y_{L'}(\Omega) [h_{l'}^{(1)}(kr) e^{i\delta_{l'}} + h_{l'}^{(2)}(kr) e^{-i\delta_{l'}}], & r > r_{MT}. \end{cases} \quad (\text{A10})$$

The eigenfunction outside the muffin-tin radius is the stationary solution appropriate for a free electron with energy $\epsilon_k = k^2/2m$ normalized within a large radius R . The phase shifts $\delta_{l'}$ are determined by matching with the solution $\phi_{L',k}^0$ inside the muffin-tin sphere. We have also introduced the lifetime η_e^{-1} of the electron due to inelastic scattering by plasmon excitation.

It is instructive to first consider the zeroth-order approximation. Using Eqs. (A3) and (A10) we obtain from Eq. (A2)

$$\epsilon_0''(\omega) = 4\pi e^2 \sum_{L_0 L'} \sum_k |P_{L_0 L'}|^2 \times \text{Im} [\epsilon_k - \epsilon_c - \omega - i(\eta_c + \eta_e)]^{-1}, \quad (\text{A11})$$

where

$$P_{L_0 L'} = \int d\vec{r} \phi_{L',k}^0(\vec{r}) (\vec{\epsilon} \cdot \vec{r}) \phi_{L_0}(\vec{r}). \quad (\text{A12})$$

We have used the form of the Green's function given by Eq. (A10) that is appropriate for $r, r' < r_{MT}$ because the core wave function ϕ_{L_0} is localized. The matrix element P implies the selection rule $|l_0 - l'| = 1$. In the limit of $\eta_c, \eta_e \rightarrow 0$, Eq. (A11) reduces to the Golden-Rule result

$$\epsilon_0''(\omega) = 4\pi^2 e^2 \sum_{L_0 L'} |P_{L',L_0}|^2 \rho(\omega + \epsilon_c), \quad (\text{A13})$$

where the electron density of state ρ is evaluated at the final-state energy $\omega + \epsilon_c$. More generally the δ function is replaced by a Lorentzian with a width given by $\eta_c + \eta_e$. We note here that in this work we have assumed that the electrons interact with a static potential $v(r)$ at each atomic site. We have included the fact that the central atom has been excited only to the extent that its muffin-tin potential, and therefore its phase shifts, are assumed to be different from the other atoms. In reality there are relaxation effects due to the screening of the central ions by the valence electrons. We assume that such screening is accomplished in a time τ which may be of the order of the inverse of the plasma frequency. On the other hand, our perturbation theory takes place over a time scale of order $(\eta_c + \eta_e)^{-1}$. Hence if the inequality

$$\eta_c + \eta_e \ll \omega_{pl} \quad (\text{A14})$$

is satisfied we may use the approximation of representing the central ion by a static screened potential. For copper the core decay rate η_c is negligible compared with η_e due to plasmon excitation,

which is of the order of 4 eV. Equation (A14) is then marginally satisfied.

Next we consider the contribution to the absorption coefficient including single scattering, i. e., first order in t . This can be obtained by a straightforward calculation of the first-order correction to the Green's function,

$$G_1^j(\vec{r}, \vec{r}') = G_c(\vec{r}, \vec{r}_1) t(\vec{r}_1 - \vec{R}_j, \vec{r}_2 - \vec{R}_j) G_c(\vec{r}_2, \vec{r}'), \quad (\text{A15})$$

and inserting the result into Eq. (A2). In performing the integrals in Eq. (A15) we note that \vec{r}_1 and \vec{r}_2 refer to the t matrix of a neighboring atom and should be outside the muffin-tin radius of the central atom. Thus we use Eq. (2.5) to expand the wave function $\Phi_{L',k}(\vec{r})$ for $r > r_{MT}$ given in Eq. (A10). Since the computation is straightforward but rather lengthy, it will not be presented here. The details are available from the authors. We would simply give the result and also point out that the expression for the Green's function propagating from one center to another has been given by Lloyd and Smith.¹⁰ Application of this expression to the multiple-scattering formalism for the present problem has been performed by Schaich⁹ and Ashley and Doniach¹³ yielding the same result. What we find is that the first-order Green's function G_1 can be expressed in terms of the matrix Z given by Eq. (2.16). Inserting G_1 into Eq. (A2) and upon comparison with the zeroth-order term we obtain

$$\chi(\omega) = \frac{\epsilon_1''}{\epsilon_0} = \frac{2 \text{Re} [\sum_{m_0} \sum_{L L'} P_{L_0, L} (\sum_j Z_{L, L'}^j) P_{L', L_0} e^{i(\delta_{l'} + \delta_{l'})}]}{\sum_{m_0} \sum_{L L'} |P_{L_0, L}|^2}, \quad (\text{A16})$$

where

$$k = \sqrt{2} [\omega + i(\eta_e + \eta_c)]^{1/2}. \quad (\text{A17})$$

If the x ray is unpolarized, then we have to average over the polarization vector, the details of which are worked out in Appendix B. In particular, if the core level is an s state then $l = l' = 1$ and $\chi(\omega)$ simply becomes

$$\chi(\omega) = \frac{1}{3} \sum_m 2 \text{Re} \left[\sum_j Z_{1m, 1m}^j(k) e^{i2\delta_1^j} \right]. \quad (\text{A18})$$

Equation (A18) is the result we shall use in this paper. Here we would only point out that if the core state is not an s state then Eq. (A16) would have

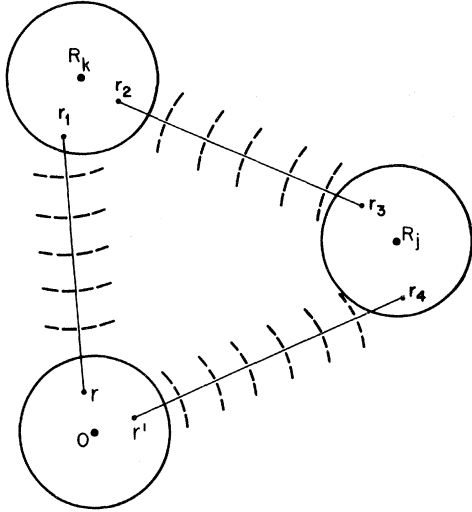


FIG. 17. Illustration of a double scattering by atoms at \vec{R}_j and \vec{R}_k .

interesting cross terms coming from the fact that the outgoing wave and the component of the incoming scattered wave may have different l values. This point will be expanded upon in a future publication.

The above result can easily be generalized to include higher-order multiple-scattering terms. The electron may be scattered first by an atom at \vec{R}_j and then an atom at \vec{R}_k . This is illustrated in Fig. 17. The corresponding correction to the Green's function is

$$G_2^{kj}(\vec{r}, \vec{r}') = G_c(\vec{r}, \vec{r}_1) t(\vec{r}_1 - \vec{R}_k, \vec{r}_2 - \vec{R}_k) \times G_0(\vec{r}_2, \vec{r}_3) t(\vec{r}_3 - \vec{R}_j, \vec{r}_4 - \vec{R}_j) G_0(\vec{r}_4, \vec{r}') \quad (\text{A19})$$

We note that the intermediate Green's function $G_0(\vec{r}_2, \vec{r}_3)$ is a Green's function for free space and can be expanded about \vec{R}_j in spherical harmonics. Then we expand the variable \vec{r}_4 about \vec{R}_j and perform the integrations as in the single-scattering case. Similarly we expand \vec{r}_1 and \vec{r}_2 about \vec{R}_k and integrate. This results in an expression for $\chi(\omega)$ of the same form as Eq. (A16) except that Z^j is replaced by

$$Z_{LL'}^{kj} = \sum_{L''L'''} Q_{LL'''}(\vec{R}_k) T_{L''L'''} K_{L''L'''}(\vec{R}_k - \vec{R}_j) \times T_{L''L'''} K_{L''L'''}(\vec{R}_j), \quad (\text{A20})$$

where

$$K_{LL_2}(\vec{R}_j) = \sum_{L_1} R_{L_2L_1}^L v_{L_1}(\vec{R}_j), \quad (\text{A21})$$

$$Q_{LL'''}(\vec{R}_k) = \sum_{L_1} v_{L_1}(-\vec{R}_k) S_{L_1L'''}^L, \quad (\text{A22})$$

and T_{LL} have been defined in Eq. (2.11). A similar expression is obtained for higher-order terms and it is clear that the expression (A16) for $\chi(\omega)$ will be valid if $\sum_j Z_{LL'}^j$ is generalized to

$$Z_{LL'}^{\text{tot}} = \sum_j Z_{LL'}^j + \sum_{j \neq k} Z_{LL'}^{kj} + \sum_{j \neq k, k \neq l} Z_{LL'}^{ljk} + \dots, \quad (\text{A23})$$

where

$$Z^{ljk \dots j} = Q(\vec{R}_1) TK(\vec{R}_1 - \vec{R}_k) T \dots TK(R_j). \quad (\text{A24})$$

Again the restriction on the sum is such that the initial and final atomic coordinate should exclude the central atom. Furthermore, the central atom should be described by a different T matrix in terms of δ'_j .

APPENDIX B

In the appendix we examine the effect of averaging over polarization vector and crystal orientation. The only dependence on the polarization vector is via the factor $\hat{\epsilon} \cdot \vec{r}$ in the matrix element. It is convenient to write

$$\hat{\epsilon} \cdot \vec{r} = \cos \theta = \frac{1}{3} \sum_m Y_{1m}^*(\Omega_1) Y_{1m}(\Omega_r), \quad (\text{B1})$$

where Ω_1 and Ω_r refer to the angle made by $\hat{\epsilon}$ and \vec{r} with respect to some axis. For polycrystalline samples we perform an average over Ω_1 and the choice of quantization axis is then arbitrary. For crystalline samples, and a given direction of the x-ray beam, however, we should average only over the azimuthal angle ϕ because the polarization vector has to be normal to the beam axis. In that case we should choose the beam axis as the quantization axis. Thus a definite direction is picked out and even with unpolarized x ray it is still possible to observe anisotropic effects. In what follows we shall work out the polycrystalline case, but the same result holds for the crystalline case provided the quantization axis is chosen as indicated. From Eq. (2.17) we write the averaged absorption rate as

$$\frac{1}{\tau} = \frac{2\pi e^2}{\hbar} 2 \text{Re} \left(\int d\Omega_1 \sum_{m_0} \sum_{L, L'} e^{i(\delta'_1 + \delta'_r)} \times \langle L_0 | \hat{\epsilon} \cdot \vec{r} | L \rangle Z_{LL'} \langle L' | \hat{\epsilon} \cdot \vec{r} | L_0 \rangle \delta(E_i + \hbar\omega - E_f) \right), \quad (\text{B2})$$

where $|L\rangle$ is the initial core state, which is coupled to the state $|L'\rangle$, which in turn is scattered by the surrounding atoms to the state $|L\rangle$. Using Eq. (B1) we can write

$$\frac{1}{\tau} = \frac{4\pi e^2}{3\hbar} \text{Re} \left(\int d\Omega_1 \sum_{m_1 m_2} Y_{1m_1}^*(\Omega_1) Y_{1m_2}(\Omega_1) \times \sum_{m_0 L L'} e^{i(\delta'_1 + \delta'_r)} \langle L_0 | r Y_{1m_1}(\Omega_r) | L \rangle \times Z_{LL'} \langle L' | r Y_{1m_2}(\Omega_r) | L_0 \rangle \delta(E_i + \hbar\omega - E_f) \right). \quad (\text{B3})$$

Using the orthogonality of the Y_{lm} we obtain

$$\frac{1}{\tau} = \frac{4\pi e^2}{3\hbar} \operatorname{Re} \left(\sum_{m_1} \sum_{m_0 L L'} e^{i(\theta_{i'} + \theta_{i''})} \langle L_0 | r Y_{1m_1}(\Omega_r) | L \rangle \right. \\ \left. \times Z_{LL'} \langle L' | r Y_{1m_1}(\Omega_r) | L_0 \rangle \delta(E_i + \hbar\omega - E_f) \right). \quad (\text{B4})$$

The case when $|L_0\rangle$ is an s wave is particularly simple. Then both $|L\rangle$ and $|L'\rangle$ are $l=1$ states and

we obtain simply

$$\frac{1}{\tau} = \frac{4\pi e^2}{3\hbar} \operatorname{Re} \left(e^{i2\theta_1} \sum_m Z_{1m,1m} \right) \\ \times |\langle l=0 | r Y_{10} | l=1, m=0 \rangle|^2 \delta(E_i + \hbar\omega - E_f). \quad (\text{B5})$$

Hence the averaged absorption rate is simply given by the average of the diagonal matrix element of Z .

*Work at the University of Washington supported in part by the National Science Foundation.

†Present address.

¹See review by L. V. Azaroff, *Rev. Mod. Phys.* **35**, 1012 (1963).

²D. E. Sayers, E. A. Stern, and F. W. Lytle, *Phys. Rev. Lett.* **27**, 1204 (1971).

³F. W. Lytle, D. E. Sayers, and E. B. Moore, Jr., *Appl. Phys. Lett.* **24**, 45 (1974).

⁴E. A. Stern and D. E. Sayers, *Phys. Rev. Lett.* **30**, 174 (1973).

⁵The original figures in Ref. 4 contain computational errors. We are grateful to the experimentalists for supplying us with the corrected data shown in Fig. 3.

⁶J. B. Pendry, *J. Phys. C* **4**, 2501 (1971); **5**, 2567 (1972); the program is listed in *Low Energy Electron Diffraction* by J. B. Pendry (Academic, New York, 1974).

⁷F. Herman and S. Skillman, *Atomic Structure Calculations* (Prentice-Hall, Englewood Cliffs, N. J., 1963).

⁸J. C. Slater, *Quantum Theory of Atomic Structure* (McGraw-Hill, New York, 1960), Vol. 1, p. 309.

⁹J. L. Beeby, *Proc. R. Soc. A* **302**, 113 (1967); the formal application of Beeby's multiple-scattering scheme to EXAFS has recently been discussed by W. L. Schaich, *Phys. Rev. B* **8**, 4028 (1973).

¹⁰P. Lloyd and P. V. Smith, *Adv. Phys.* **21**, 69 (1972).

¹¹D. E. Sayers, thesis (University of Washington, 1971) (unpublished).

¹²J. L. Beeby, *J. Phys. C* **1**, 82 (1968).

¹³C. A. Ashley and S. Doniach, *Phys. Rev. B* **11**, 1279 (1975).

¹⁴R. de L. Kronig, *Z. Phys.* **70**, 317 (1931); **75**, 191 (1932); **75**, 468 (1932).

¹⁵E. A. Stern, *Phys. Rev. B* **10**, 3027 (1974).